Feasibility of achieving gain in transition to the ground state of C VI at 3.4 nm

Yoav Avitzour and Szymon Suckewer

Princeton University, Princeton, New Jersey 08540 USA

Received August 4, 2006; revised November 29, 2006; accepted November 29, 2006; posted December 8, 2006 (Doc. ID 73735); published March 15, 2007

We present numerical studies of recombination gain in the transition to the ground state of H-like C ($2\rightarrow1$ transition at $\lambda=3.4$ nm). It is shown that high gain (up to about 180 cm^{-1}) can be achieved using currently available, relatively compact, laser technology. The model includes the ionization of the plasma by an ultraintense, ultrashort laser pulse, followed by plasma expansion, cooling, and recombination. Transient population inversion is generated during the recombination process. We investigate the behavior of the gain with respect to different plasma parameters and pump pulse parameters and explain how the different properties of the plasma and the pump pulse affect the gain.

OCIS codes: 020.2070, 140.3210, 140.7090, 140.7240, 260.3230, 350.5400.

1. INTRODUCTION

Since the concept was first introduced in the early 1970s,[1,2] the idea of recombination scheme x-ray lasers was attractive due to its potential of achieving lasing at very short wavelengths with relatively moderate pumping requirements. Particularly so when using a recombination-to-ground-state scheme in H-like ions, in which the lasing transition energy constitutes a large portion (3/4) of the overall ionization energy. During the 1990s a couple of experiments demonstrated gain,[3,4] which was then followed by demonstration of lasing action,[5,6] in the $2\rightarrow1$ transition of Li III ions. Alongside the experimental efforts, several theoretical studies were conducted to identify the processes involved in gain creation and to characterize the initial conditions required to achieve gain in a recombination scheme.[7–10]

Recently, we developed an elaborate numerical model to characterize recombination gain in the $2\rightarrow1$ transition of Li III at 13.5 nm.[11,12] The model describes the effects of different experimental parameters on the gain. We were able to explain the gain observed in the above-mentioned experiments[5,6] and showed that it is possible to achieve high gain in this transition, especially when mixing the plasma with hydrogen.

Recombination gain relies on having fully stripped ions in a relatively cold plasma. The ionization mechanism that is used to achieve this plasma is tunneling ionization by ultrashort (with pulse duration of $\tau\lesssim100$ fs), ultraintense (with intensity of approximately 10^{17} to 10^{19} W/cm^2, depending on the element used) laser pulses. Due to the short pulse duration, minimal heating is produced during ionization. However, when calculating the average energy that is absorbed during the ionization process, we find that the absorbed energy still corresponds to an electron temperature that would not allow for population inversion in the transition to ground state to be generated during the recombination process. This is in contrast to the above-mentioned experiments, which demonstrated gain in the transition to the ground state of Li III. We have shown[11] that taking into account the actual phase-space distribution function of the plasma, including effects from both the non-Maxwellian nature of the distribution function and the spatial expansion and cooling of the plasma after ionization, high gain is indeed feasible in the Li III $2\rightarrow1$ transition. In addition, we have shown more recently[12] that the gain can be enhanced and become less stringently dependent on exactly matching the required values of the experimental parameters, if hydrogen is mixed into the plasma.

As we mentioned above, the main advantage of using a recombination-to-ground-state scheme is the favorable scaling of the required pumping energy (in comparison to other schemes) when going to shorter wavelengths. A highly desirable wavelength range is the so-called "water window," which is in the range between 2.3 and 4.4 nm, for which absorption in water is very low. An x-ray laser with a wavelength in this range could be used for a multitude of applications, e.g., high-resolution imaging of "wet" biological samples. For the $2\rightarrow1$ transition of H-like ions, the first element that reaches this range is carbon (C VI), with the $2\rightarrow1$ transition wavelength at $\lambda=3.4$ nm. We present calculations for the recombination gain in this transition.

The basic scheme for recombination x-ray lasers is the same regardless of the ion used. A schematic setup is presented in Fig. 1. An ultrahigh power, ultrashort laser pulse (the "pump" pulse) is focused by lens L1 into a high-density gas (or low-ionized plasma—see below) and completely strips the ions of their electrons through optical field ionization (OFI), to achieve a relatively cold, fully stripped plasma.[7] The pump may be preceded by a so-called "prepulse" to create an initial plasma ("preplasma") to provide better guiding for the propagation of the pump pulse in the plasma. Since the pump pulse is very short, minimal heating is induced in the plasma during ionization, and rapid recombination and de-excitation processes

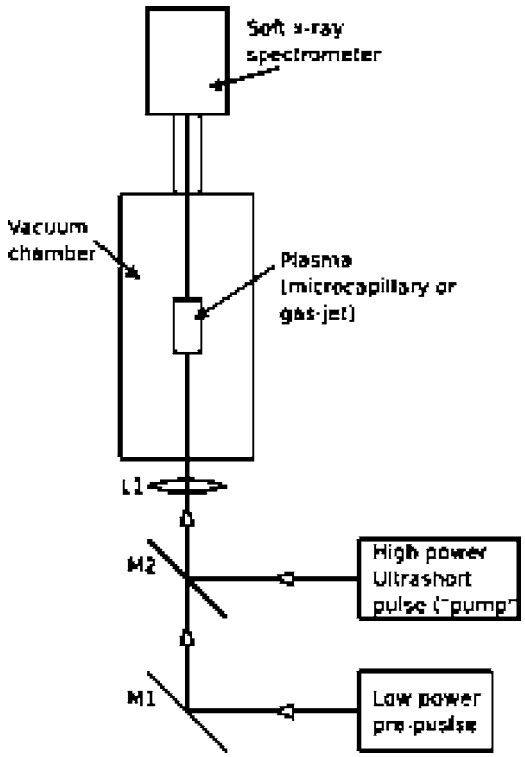

Fig. 1. Schematic setup for a recombination laser experiment.

follow, governed by three-body recombination and electron-impact de-excitation (due to the high plasma density). During the recombination process, given certain initial conditions (discussed below), transient population inversion can be created.

The process of gain generation can be divided into three stages: (a) ionization and heating, (b) expansion and cooling, and (c) recombination and gain. We will repeat briefly the principles of our model (described in detail in Refs. 11 and 12) and discuss more deeply the adjustments and enhancements that were required in order to apply the model to the current, higher-Z ion.

2. IONIZATION AND HEATING

Ionization is achieved by OFI using an intense laser pulse. The ionization rate is calculated by the tunneling rate of an electron under the influence of the laser electric field treated in a semiclassical approximation[13,14]

$$W_{st} = \frac{\omega_0}{2}\frac{U_Z}{U_h}\frac{(2l+1)(l+|m|)!}{2^{|m|}(|m|)!(l-|m|)!}\left(\frac{2e}{n^*}\right)^{2n^*}\frac{1}{2\pi n^*}\frac{U_Z}{U_h} \times\left[2\left(\frac{U_Z}{U_h}\right)\frac{E_{h,0}}{E}\right]^{2n^*-|m|-1}\exp\left[-\frac{2}{3}\left(\frac{U_Z}{U_h}\right)^{3/2}\frac{E_{h,0}}{E}\right], \quad (1)$$

where here e is the natural exponent, n^* is the effective principal quantum number, given by $n^*=Z\sqrt{U_Z/U_h}$, ω_0 is the atomic frequency unit of 4.1×10^{16} s^{-1}, U_Z and U_h are the ionization potentials of the ion and of a hydrogen atom, respectively, $E_{h,0}$ is the atomic field strength at the first Bohr radius of hydrogen ($E_{h,0}=5.1\times10^9$ V/cm), and E is the laser electric field. This expression is valid when $(U_Z/U_h)^{3/2}E_{h,0}/E \ll 1$.

The classical motion of the ionized electrons in the laser field after ionization yields the so-called residual energy that is absorbed by the electrons during the ionization process. This energy is due to the phase mismatch between the ionized electrons and the oscillating laser electric field.[15] It is proportional to the quiver energy of the electrons at the time of ionization, given by

$$\mathcal{E}_q(t) = \frac{e^2E(t_0)^2}{4m_e\omega^2}, \quad (2)$$

where $E(t_0)$ is the laser electric field amplitude at the time of ionization and ω is the laser angular frequency. Though the residual energy is in fact much smaller than the quiver energy, it could be high enough to prevent gain creation if the plasma were Maxwellian. However, the ultrashort ionization process yields a plasma with a highly non-Maxwellian distribution function as was shown before.[11,12,16] We will not repeat the quantitative demonstration of the non-Maxwellian nature of the electron distribution function (EDF) of the OFI plasma, but qualitatively, one can understand the properties of the OFI EDF by realizing that most of the electrons are ionized at the peak of the oscillating electric field and continue to move in phase with it. Therefore, the vast majority of the electrons in the plasma absorb very little residual energy, and only a small fraction of the electrons are ionized off the peak of the laser electric field and absorb high energy. These highly energetic electrons contribute much to the overall electron average energy, but have a relatively low probability of participating in collisional processes. This effect gives rise to enhanced three-body recombination and electron-impact de-excitation rates. In other words, the non-Maxwellian nature of the distribution function causes the "effective recombination temperature" of the plasma to be much lower than the temperature of the corresponding Maxwellian plasma, given by $\frac{2}{3}$ of the average energy. The "effective recombination temperature" can be defined by comparing the actual three-body recombination rate to the same rate in a Maxwellian plasma. This definition is not unique, since one has to decide which recombination rate to compare. In any case, the effective recombination temperature is always significantly lower for an OFI plasma than for a Maxwellian plasma with the same average energy.

The ionization was simulated by the iPIC (ionization particle in cell) code, developed and described in Ref. 11 with enhancements described in Ref. 12. The iPIC code is a 1D electrostatic code that calculates the plasma in a cross section of the propagation of the laser; i.e., the dimension of the calculation is the transverse dimension. The code includes ionization as well as binary collisions, and typically runs in parallel on 10 dual CPU nodes on the Princeton Plasma Physics Laboratory (PPPL) Scientific Computing Cluster. The reasons that a 1D code has to run in parallel are the severe restrictions on the time step (resolving the laser frequency), the cell size (high-density low-temperature plasma), and the need for a large number of particles to maintain good statistics when using Monte Carlo methods for both ionization and

binary collisions. All of the physics and the numerical methods described before were developed for H-like ions, therefore the same tools that were initially developed for the study of H-like Li III ions were available to study H-like C VI ions as well, with some necessary modifications as described below.

For a sufficiently high electron density ($n_e \geqslant 5 \times 10^{19}$ cm^{-3}), and a fixed electron temperature, gain is higher for higher-Z ions, as discussed in Section 4. Therefore, we can expect to get better results for C VI ($Z=6$) than for Li III ($Z=3$). However, the required intensity for the ionization of C VI ions is almost 2 orders of magnitude higher than the intensity required to ionize Li III ions, and with it, the average energy of the electrons. The effects of the residual energy on the recombination gain are reduced significantly when taking into account the non-Maxwellian nature of the distribution function and by adding hydrogen to the plasma as shown in Ref. 12. Adding hydrogen supplies cold electrons to the plasma since the hydrogen atoms are ionized by the front of the pump pulse (or by the pre-pulse) and absorb very little residual energy. These electrons then participate in the recombination process and enhance the gain. In the C VI case, however, higher densities are required to achieve gain (about an order of magnitude higher than that required for Li III, see Section 4), and collisions during the ionization process become more significant since the collision frequency scales linearly with the density. Unlike the residual heating, collisional heating affects the electrons that were ionized from carbon (C electrons) and the electrons ionized from hydrogen (H electrons) in the same way. One way to counter this effect is to use a much shorter pulse as a pump. The overall collisional heating is roughly proportional to the product $\nu_{col}\tau$, where ν_{col} is an average collision frequency, and τ is the pulse duration. Therefore, increasing the density (and with it the collision frequency) by a factor of 5–10 and reducing the pulse duration by the same factor should have very little net effect on the collisional heating. Ultrahigh intensity laser pulses of the order of 10–20 fs are currently available at university scale labs. With recent advances in the nonlinear Raman backscattering amplification and compression technique,[17,18] it is expected that a compact, ultrahigh power system that would deliver pulses with the required intensity and pulse duration, will be available in the near future. Using shorter pump pulses requires one to use a slightly higher intensity, since the ionization has to be completed in a shorter time, and *full* ionization is crucial to achieve high gain. However, even with the higher intensity, the shorter pulses still contain lower energy, which means that using shorter pulses would be more energy efficient. The energies and intensities required for different pumping pulse durations are detailed in Table 1.

The effects of higher density and higher intensity leading to higher residual energy described here are essentially the same effects that were studied in the lower-Z case. The main difference is that the higher intensity not only increases the residual energy, but also introduces some of the effects that were not significant for lower-Z ions. First, the electron quiver velocity under the influence of the laser is high enough that relativistic effects from the relativistic motion of the electrons oscillating in the laser field are significant. The other effect, which turned out to be more significant than the pure relativistic effects, is the electric ponderomotive force, f_p, given by

$$f_p = \frac{e^2}{4m_e\omega^2}\nabla|\vec{E}|^2, \tag{3}$$

where $\vec{E}$ is the laser electric field. The ponderomotive force, which is proportional to the pump laser intensity and inversely proportional to the pump beam diameter, creates a large charge separation in the plasma, followed by oscillations that cause additional heating. Therefore, aiming for small pump beam radii, which yielded the highest gain for the Li III case, is no longer the best strategy. The effect of the ponderomotive force can be roughly estimated by comparing it to the self-consistent electric force in the plasma f_s (Ref. 11),

$$\frac{f_s}{f_p} \sim 6\frac{\tilde{n}_e}{\tilde{I}}\left(\frac{r_0}{\lambda}\right)^2\frac{\delta n_e}{n_e}, \tag{4}$$

where f_p is evaluated here by its maximum value assuming a Gaussian beam profile with radius r_0 [$E \sim E_0 \exp(r/r_0)^2$], pump beam wavelength λ, pump intensity $\tilde{I}$ (in units of 10^{17} W/cm^2), and electron density $\tilde{n}_e$ (in units of 10^{19} cm^{-3}). The term $\delta n_e/n_e$ represents the density fluctuations that are induced by the ponderomotive force. Since these density fluctuations create in turn a strong restoring self-consistent electric force, the maximum fluctuations that can be induced by the ponderomotive force must satisfy $f_s/f_p \leqslant 1$. For the Li III case, with $\tilde{I}=1$, $\tilde{n}_e=1$, and a typical value for r_0/λ of approximately 5 (for a tightly focused beam), we see that the ponderomotive force would induce density fluctuations of no more than 1%, and would therefore be negligible. However, keeping all other parameters the same and increasing $\tilde{I}$ by 2 orders of magnitude would allow for fluctuations of nearly 100%, turning the influence of the ponderomotive force to one of the significant factors that limit the gain. This effect is reduced somewhat by the higher electron density that is required to achieve gain in C VI, but it remains a significant effect.

Finally, the higher electron density causes the time at which gain is achieved and the gain duration to be much shorter than in the case of lower-Z elements, due to higher collision frequency. Clearly this also means faster Maxwellization, yet since the Maxwellization of the hot

Table 1. Pump Intensities Used for the Different Pulse Durations and Corresponding Pulse Energies[a]

	Pulse Duration		
	$\tau=10$ fs	$\tau=20$ fs	$\tau=50$ fs
Peak intensity (W/cm^2)	10^{19}	8×10^{18}	6.5×10^{18}
Pulse energy (mJ) for $r_0=10$ μm	100	160	32

[a]These are the minimum intensities required to achieve *full* ionization of carbon.

electrons is slower than that of the cold electrons, gain may still be generated before Maxwellization effects take place.

The iPIC code was modified to numerically integrate the relativistic equation of motion and Lorentz force for a particle in three dimensions in velocity and one spatial dimension (where as before, the spatial dimension is aligned along the polarization of the laser electric field). The numerical scheme is based on the one presented in Ref. 19.

3. EXPANSION AND COOLING

The expansion and cooling (along with Maxwellization) process is simulated by numerically solving the Fokker–Planck (FP) equation for the distribution function that is calculated by the iPIC code. The code used is the same FP solver we used before,[11,12] which is an implementation of the SPARK code,[20] described in detail in Ref. 21. The code solves the 1D FP equation in the diffusive approximation, which includes the collisional effects in the plasma.

One of the problems that arose when applying to C VI ions the tools that were developed for the Li III ions was the transition from the iPIC code to the FP solver. Due to the ponderomotive force, space-charge separation is created in the plasma by the laser, and space-charge oscillations follow. For higher plasma densities, these oscillations are damped out very quickly (in time scales shorter than the pulse duration), but for lower plasma densities and tightly focused beams, the oscillations continue for longer times. Since the FP code solves the FP equation in the diffusive approximation, it cannot handle such oscillations. The solution was to insert into the FP solver a plasma-frequency-averaged distribution function after ionization produced by the iPIC code. Figure 2 shows snapshots of the plasma after ionization. The oscillations are seen clearly, and very different results would be obtained, for example, if we inserted the distribution function from Fig. 2(c) or from Fig. 2(d) as an initial condition for the FP solver code. Averaging over one plasma period added the excess space-charge oscillation energy to the plasma and gave results that were independent of the exact moment after the ionization in which a snapshot of the distribution function was taken. (See Fig. 3.) Since the OFI EDF was generated by the iPIC code in planar geometry, and since the charge separation and space-charge oscillations may not have cylindrical symmetry (recall that the pump beam is linearly polarized), the straightforward conversion between planar and cylindrical symmetries that was used before[11,12] was no longer appropriate here, and the planar geometry option of the FP solver code was used.

Finally, we note that due to the higher density and the short time scales at which gain occurs (usually less than 1 ps after ionization), the expansion cooling plays a less important role here since very little expansion can happen in these time scales. (The main importance of solving the FP equation is for calculating the Maxwellization pro-

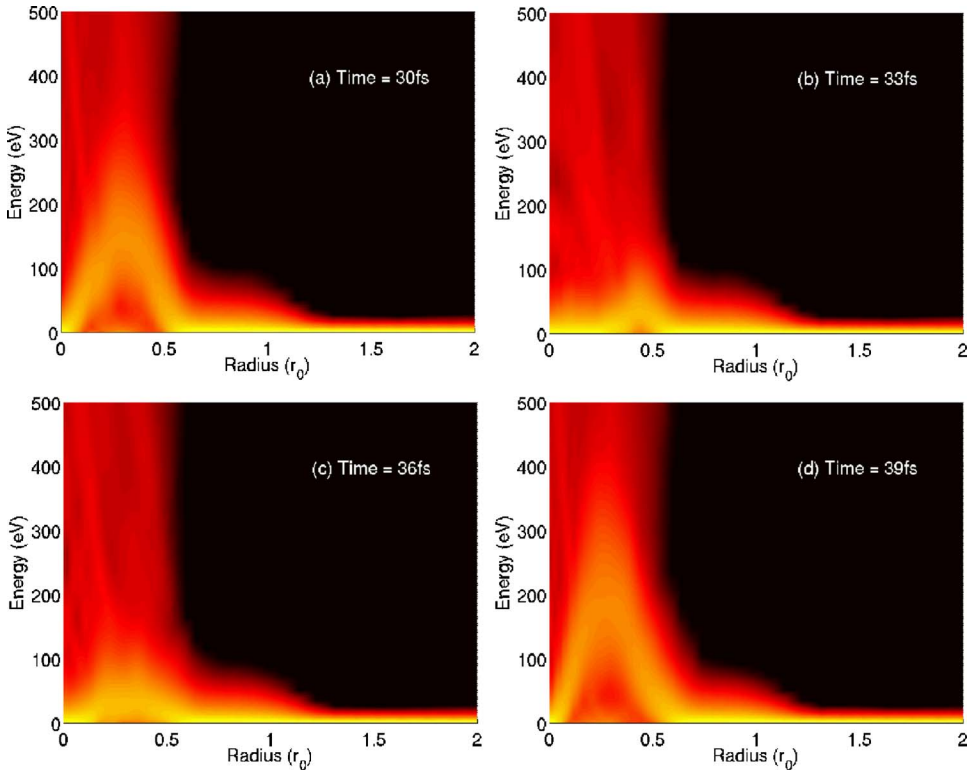

Fig. 2. (Color online) Snapshots of the distribution function after ionization at different times during one plasma cycle. The distribution function (in arbitrary units) is presented as a function of radius (in units of the beam radius, r_0) and energy (in electron volts). The space-charge oscillation is seen going from parts (a) to (d). The calculation was done for C and H densities $n_C=10^{19}$ cm^{-3}, $n_H=5\times10^{19}$ cm^{-3}, respectively, pump laser wavelength of $\lambda=400$ nm, beam diameter of $d=10$ μm, pulse duration of $\tau=20$ fs, and peak intensity of $I_p=8\times10^{18}$ W/cm^2. The plasma cycle for the above parameters (for fully ionized plasma) is $T_p=2\pi/\omega_p\approx10$ fs. The snapshots are given every 3 fs starting from 30 fs, where 0 is defined at the peak of the pulse.

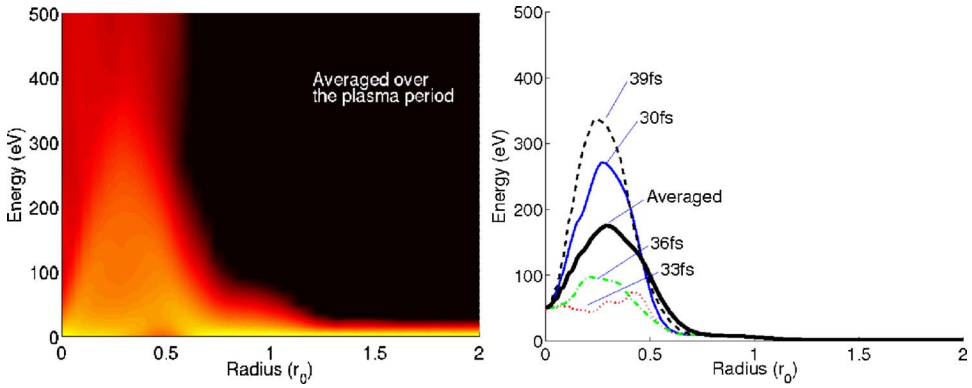

Fig. 3. (Color online) Distribution function and average energy averaged over one plasma cycle. On the left: the plasma-cycle-averaged electron distribution function (in arbitrary units) as a function of radius (in units of beam radius, r_0) and energy (in units of electron volts). On the right: plots of the average energy of the electron versus radius. The average energies of the distribution functions given in Fig. 2 are plotted, along with the cycle-averaged average energy. All of the simulation parameters are the same as those for Fig. 2

cess, which has to be taken into account to get realistic results.) Therefore, in contrast to the Li III case, there is no need for a tight focus of the pump pulse in order to achieve gain (other than for achieving the required intensity). This property of the gain may help in achieving longer gain channels and reaching gain saturation.

4. RECOMBINATION AND GAIN

The recombination process was simulated by solving the rate equations governing the process, taking into account all the relevant atomic (ionic) processes that take place. These include three-body recombination, electron-impact ionization, electron-impact excitation and de-excitation, radiative recombination, and radiative relaxation (spontaneous emission). The plasma was assumed to be optically thin and the calculation was for small-signal gain, hence no photoexcitation processes were considered. The rate equations are given by

$$\frac{dn_k^{Z+}}{dt} = n_e \sum_{m\neq k} \beta_{mk}^{Z+} n_m^{Z+} - n_e n_k^{Z+} \sum_{m\neq k} \beta_{km}^{Z+} + \sum_{m>k} A_{mk}^{Z+} n_m^{Z+} - n_k^{Z+} \sum_{m<k} A_{km}^{Z+} + \delta_{k,1} n_e \sum_m S_m^{(Z-1)+} n_m^{(Z-1)+} - n_e S_k^{Z+} n_k^{Z+} + \alpha_k^{Z+} n_e n_1^{(Z+1)+} - \delta_{k,1} n_e n_k^{Z+} \sum_m \alpha_m^{(Z-1)+}, \quad (5)$$

where

- n_k^{Z+} is the number density of the kth principal quantum level of $Z+$ ions,
- β_{km}^{Z+} is the collisional (de)excitation rate between principal quantum levels k and m of the $Z+$ ions,
- A_{km}^{Z+} is the Einstein A coefficient for spontaneous emission during a $k \rightarrow m$ transition in a $Z+$ ion ($k > m$),
- S_k^{Z+} is the electron-impact ionization rate from the kth level of a $Z+$ ion,
- α_k^{Z+} is the overall recombination rate *into* the kth level of a $Z+$ ion, $\alpha_k^{Z+} = \alpha_{k,rad}^{Z+} + n_e \alpha_{k,3body}^{Z+}$, where $\alpha_{k,rad}$ is the radiative recombination rate and $\alpha_{k,3body}^{Z+}$ is the three-body recombination rate.

The values of the above rates were obtained by integrating the cross sections of the different interactions over the actual non-Maxwellian, time-dependent, electron-distribution function that was obtained from the iPIC and FP codes. (See Ref. 12 for more details.) The small-signal gain coefficient was then calculated from

$$G_{u\rightarrow l} = n_u \sigma_{ul} \mathcal{F}, \quad (6)$$

where u and l are the upper and lower lasing levels, respectively, $\mathcal{F} = 1 - (n_l g_u)/(n_u g_l)$, and

$$\sigma_{ul} = \frac{\pi r_e f_{lu} \lambda}{\Delta\lambda/\lambda} \frac{g_l}{g_u} \mathcal{L}_\lambda(\lambda), \quad (7)$$

where $\mathcal{L}_\lambda(\lambda)$ is a dimensionless line-shape function with linewidth $\Delta\lambda$. The line shape and width were estimated using the Voigt profile of the line, combining the estimated Doppler broadening for the cold ions. The ions were assumed to be fixed during the whole process, hence the ions' temperature was taken to be the initial plasma temperature, i.e., $T_i \sim 1$ eV. Although the actual temperature of the ions may rise during the ionization and recombination process, it is not expected to have a large effect on the gain due to the following: the main broadening mechanism for such high densities is Stark broadening, Doppler broadening scales like $\sqrt{T_i}$, and ion heating due to inverse-brehmstrahlung absorption ion heating is not expected to be very high, since the laser is very short. Whereas collisions already play a secondary role in the heating of the plasma, the electron-ion collision frequency is much smaller than the electron–electron collision frequency, since the electron cloud moves very rapidly around the stationary ions, while the relative velocities between the electrons are small. The Stark broadening is estimated for the Lyman-α line by the lesser of the widths given by the quasi-static linear Stark effect (Holtsmark theory) and electron-impact broadening.[22,23]

To understand how the gain behaves for different ions, we provide first both an analytical and numerical analysis of the rate equations (5) using temperature-dependent rates.

We start by rewriting the rate equations (5) in a more convenient form. We look only at the first stage of recombination, i.e., recombination into the H-like ion and neglect the next stage of recombination into the He-like ion. This, in general, reduces the gain since recombination

from the ground state of the H-like ion into the He-like ion state will decrease the ground-state population and increase the gain, but this is usually small in the time scales of interest. Let $\mathbf{n}$ be a vector of the populations of the different H-like ion levels:

$$\mathbf{n} = \begin{pmatrix} n_1 \\ n_2 \\ \vdots \\ n_K \end{pmatrix}, \tag{8}$$

where K is the maximum principal quantum number taken into account in the calculation determined by the density.[24] Let n^0 be the population of the fully ionized ions, and let n_e be the electron density. The rate equations (5) can then be written as

$$\frac{d\mathbf{n}}{dt} = n_e^2 n^0 \boldsymbol{\alpha} - n_e(\mathrm{diag}(\mathbf{S} + \beta \cdot \mathbf{1}) + \beta^t) \cdot \mathbf{n} + (A^t - \mathrm{diag}(A \cdot 1)) \cdot \mathbf{n} \equiv n_e^2 n^0 \boldsymbol{\alpha} + n_e \hat{a} \cdot \mathbf{n} + \hat{b} \cdot \mathbf{n},$$

$$\frac{dn^0}{dt} = \frac{dn_e}{dt} = -n_e^2 n^2 \boldsymbol{\alpha} \cdot \mathbf{1} + n_e \mathbf{S} \cdot \mathbf{n}, \tag{9}$$

where $\boldsymbol{\alpha}$ is the three-body recombination rate vector, with α_k being the three-body recombination rate to level k [radiative recombination was neglected here since $\alpha_{rad} \ll \alpha_{3\mathrm{body}}$ for the electron densities ($n_e > 10^{18}$ cm^{-3}) and temperatures ($T_e < 50$ eV) considered here]; A is the Einstein A coefficients matrix, where A_{km} is the spontaneous emission rate between level k to level m ($k > m$), and $A_{km} = 0$ for $k \leqslant m$; $\mathbf{S}$ is the impact ionization rate vector, where S_k is the impact ionization rate from level k; β is the impact (de)excitation rate matrix, where β_{km} is the impact (de)excitation rate from level k to level m; $\mathbf{1}$ is a column vector of 1's of length K, useful for writing algebraically the operation of summing up elements of a vector, and the operator diag[$\mathbf{x}$] creates a diagonal matrix with the elements of the vector $\mathbf{x}$ on its diagonal. The matrices $\hat{a}$ and $\hat{b}$ are defined by Eq. (9). We proceed by arguing that in the time scales of interest (a few picoseconds after ionization), only a small fraction of ions recombine, therefore

$$\left| \frac{1}{n_e} \frac{dn_e}{dt} \right| = \left| \frac{1}{n^0} \frac{dn^0}{dt} \right| \ll 1, \tag{10}$$

such that to the zeroth order we can neglect the variation in n_e and n^0. We can now rewrite Eq. (9) in the canonical linear ODE form

$$\frac{d\mathbf{n}}{dt} \approx \mathcal{A} \cdot \mathbf{n} + \mathbf{B}, \tag{11}$$

where $\mathcal{A} = n_{e0}\hat{a} + \hat{b}$ and $\mathbf{B} = n_{e0}^2 n_0^0 \boldsymbol{\alpha}$. Simplifying further, we look at the two-level system, taking into account only the ground state and the first excited state of the H-like ion. Equation (11) becomes

$$\begin{pmatrix} \dot{n}_1 \\ \dot{n}_2 \end{pmatrix} = \begin{bmatrix} -n_e(\beta_{12} + S_1) & n_e\beta_{21} + A_{21} \\ \beta_{12} & -n_e(\beta_{21} + S_2) - A_{21} \end{bmatrix} \begin{pmatrix} n_1 \\ n_2 \end{pmatrix} + n_e^2 n^0 \begin{pmatrix} \alpha_1 \\ \alpha_2 \end{pmatrix}. \tag{12}$$

Assuming that we are in a recombination-dominated regime (low electron temperature), we can neglect all ionization, and assume that $\beta_{12} \ll \beta_{21}$. Matrix $\mathcal{A}$ can be rewritten in the following way:

$$\mathcal{A} \approx \theta \begin{bmatrix} -\xi & 1 \\ \xi & -1 \end{bmatrix}, \tag{13}$$

where $\theta = n_e\beta_{21} + A_{21}$ and $\xi = n_e\beta_{12}/(n_e\beta_{21} + A_{21})$. This system can be easily solved analytically. We interested in the $2 \to 1$ gain coefficient, which is proportional to $n_2 - 4n_1$. Solving Eq. (12) and Eq. (13) gives

$$G \sim n_2 - 4n_1 = \frac{5}{\theta}(\xi B_1 - B_2)(e^{-\theta(\xi+1)t} - 1) - (1 - \xi) \times \left[\exp\left(\frac{B_1 + B_2}{1 + \xi} t \right) - 1 \right]. \tag{14}$$

For $\xi \ll 1$, we get

$$G \sim \frac{5B_2}{\theta}(1 - e^{-\theta t}) - (e^{(B_1+B_2)t} - 1). \tag{15}$$

It is clear from analysis of Eq. (15) that $G(0) = 0$ and $G(t \to \infty) \to -\infty$ (taking the limit to ∞ is invalid under the assumptions of this derivation, however the meaning of this is that, at most, there is a limited time for which $G > 0$). The time of maximum gain is found by solving $dG/dt = 0$:

$$t_{\max} = \frac{1}{B_1 + B_2 + \theta} \ln \frac{5B_2}{B_1 + B_2}. \tag{16}$$

A simple analytic form of the three-body recombination rate is given by

$$\alpha_k = \frac{C g_n n^2}{Z^2 T^2} \exp\left(\mathrm{Ryd} \frac{z^2}{n^2 T^2} \right) \mathcal{E}_1\left(\frac{\mathrm{Ryd}\, Z^2}{n^2 T^2} \right), \tag{17}$$

where $\mathcal{E}_1(x) = \int_x^\infty e^{-t}/t\,dt$ is the exponential integral function defined for $x > 0$. (This rate is obtained by first finding an effective three-body recombination "cross section" using the detailed balance relation for the well-known Lotz impact ionization cross section[25] and then integrating over a Maxwellian distribution function, see, e.g., Ref. 16.) The maximum gain is given by

$$G_{\max} \equiv G(t = t_{\max}) \sim 1 + 5\delta(1 - (5\gamma)^{-\gamma/(\delta+\gamma)}) - (5\gamma)^{\delta/(\delta+\gamma)}, \tag{18}$$

where $\gamma \equiv \alpha_2/(\alpha_1 + \alpha_2) \sim 1$ for all relevant values of T_e and Z ($T_e < 50$ eV, $Z < 10$), and $\delta \equiv B2/\theta = n_e^2 n^0 \alpha_2/(n_e\beta_{21} + A_{21})$. β_{21} is given by (Obtained similarly by from the detailed balance relation applied to the impact-excitation cross section given in Ref. 26.)

$$\beta_{21} \approx \frac{4.44 \times 10^{-7}\,\mathrm{cm}^3}{\mathrm{Ryd}\,Z^2\sqrt{T}}\frac{}{\mathrm{s}}. \tag{19}$$

Evaluating Eq. (17) for α_2 gives

$$\alpha_2 \sim 8 \times 10^{-45}\frac{1}{\mathrm{Ryd}\,Z^2T^2}\exp\left(\frac{\mathrm{Ryd}\,Z^2}{4T^2}\right)\mathcal{E}_1\left(\frac{\mathrm{Ryd}\,Z^2}{4T^2}\right)\frac{\mathrm{cm}^6}{\mathrm{s}}, \tag{20}$$

and the spontaneous emission coefficient is given by

$$A_{21} = 3.36 \times 10^6\,\mathrm{Ryd}\,Z^2. \tag{21}$$

Combining Eqs. (19)–(21) gives the following expression for δ:

$$\delta \approx 2\frac{\tilde{n}_e\tilde{n}^0}{T^{3/2}}\exp\left(\frac{\mathrm{Ryd}\,Z^2}{4T^2}\right)\mathcal{E}_1\left(\frac{\mathrm{Ryd}\,Z^2}{4T^2}\right), \tag{22}$$

where $\tilde{n}_e = n_e \times 10^{-19}\ \mathrm{cm}^3$ and $\tilde{n}^0 = n^0 \times 10^{-19}\ \mathrm{cm}^3$. Typical values for δ are in the low-temperature limit ($T \sim 1$ eV), the exponential terms in (22) are dominant, and typical values of *delta* are of order 10^{-2} to 10^{-3}. The final result for $G_{\max}$ for $\gamma \sim 1$ and $\delta \ll 1$ is

$$G_{\max} \sim 2.4\delta. \tag{23}$$

Since the analytical analysis given above is not sufficient to get a qualitative parameter range for which gain is feasible, numerical integration of the rate equations (5) using temperature-dependent rates is presented in Fig. 4. Gain (in cm^{-1}) was calculated as a function of temperature and atomic number, Z, for four different densities of pure elements.

Several trends can be identified by studying the figures. First, as expected, gain is very high for very low temperatures and drops substantially when the temperature is increased. For $T_e > 10$ eV, gain can be obtained only for high Z and very high density. Second, for a high enough density, gain is higher for higher Z. This trend is explained by two properties of the system. First, there is a factor of Z^2/T^2 in Eq. (22), which allows for higher temperatures to yield gain in higher Z. This factor, however, is not affecting the gain strongly and the gain is still limited by an overall factor of $T^{-3/2}$. The other reason gain is higher for the higher-Z case is that since the density parameter in the simulations was the ion density, increasing Z also increases the electron density by a factor of Z, which in turn increases the gain by a factor of Z^2. More interesting, however, is that this behavior is only observed when the initial ion density is high enough. This is most likely due to the requirement that the recombination process and gain occur on a much shorter time scale for higher-Z ions (the spontaneous emission coefficient has a Z^2 scaling as well), and the time scales of the recombination process and the gain are determined mainly by the density. Specifically for C VI, we see that a minimum density of 5×10^{19} is required to achieve gain. How-

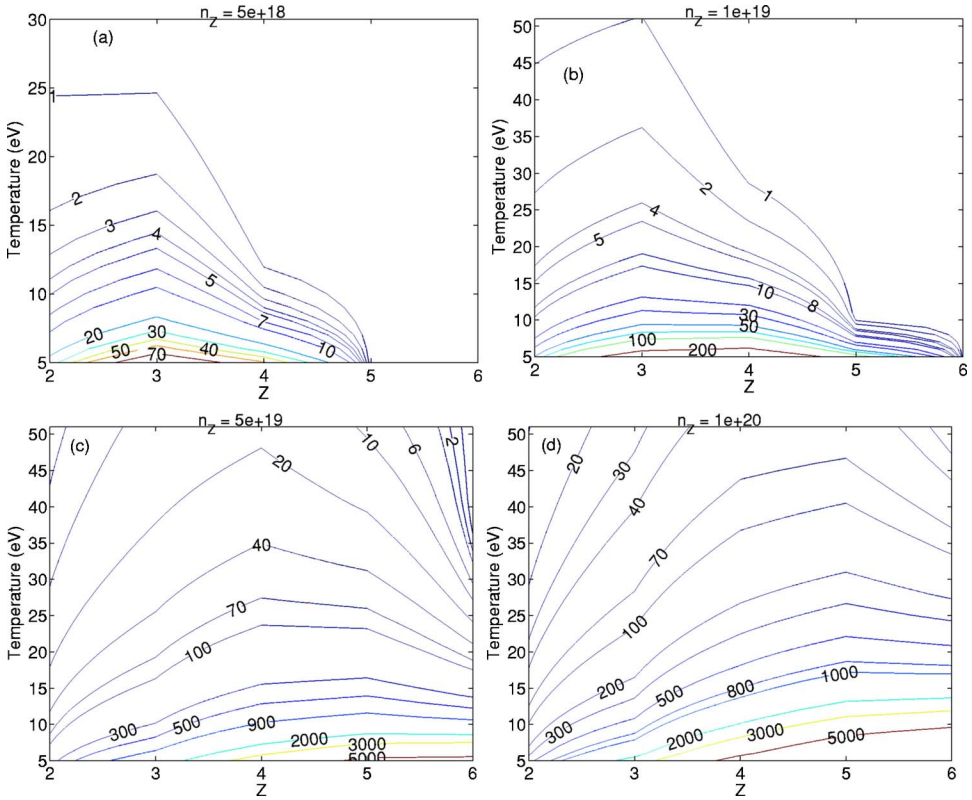

Fig. 4. (Color online) Logarithmic contour plots of the maximum gain coefficient (cm^{-1}) for the $2 \rightarrow 1$ transition calculated using temperature-dependent rates. Gain is given as a function of temperature and atomic number, for four different ion densities (given in units of cm^{-3}) (a) 5×10^{18}, (b) 1×10^{19}, (c) 5×10^{19}, and (d) 1×10^{20}.

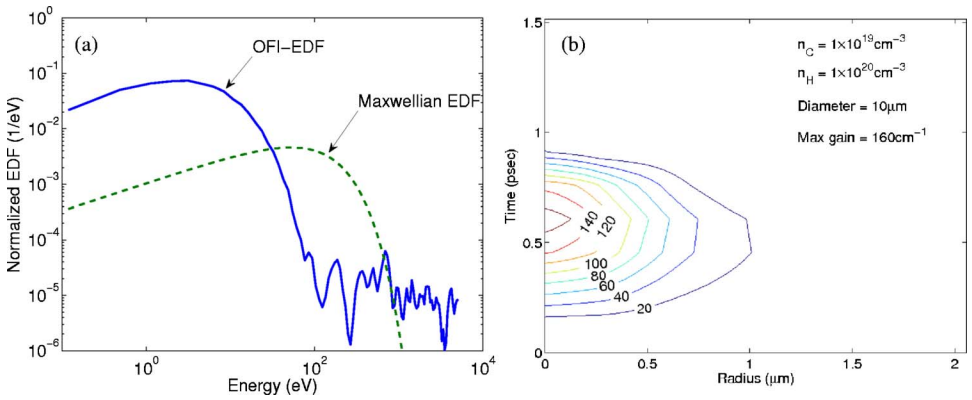

Fig. 5. (Color online) Calculated results for carbon density of $n_C=10^{19}$ cm^{-3}, hydrogen density of $n_H=10^{20}$ cm^{-3}, pump beam diameter of $d=10$ μm, wavelength of $\lambda=400$ nm, pulse duration of $\tau=20$ fs, and peak pump intensity of $I_p=8\times10^{18}$ W/cm^2. (a) Comparison of the OFI-EDF and Maxwellian distribution function with the same average energy. (b) Gain in CVI ions with hydrogen added. Gain is presented in units of cm^{-1} versus time and space.

ever, once this density has been reached, gain is higher for higher-Z ions, when the temperature is fixed.

5. RESULTS

A typical result from the numerical model described above for the C VI case is presented in Fig. 5. This calculation was performed for carbon density of $n_C=10^{19}$ cm^{-3}, hydrogen density of $n_H=10^{20}$ cm^{-3}, pump beam diameter of $d=10$ μm, pump beam wavelength of $\lambda=400$ nm, pump pulse duration of $\tau=20$ fs, and peak intensity of $I_p=8\times10^{18}$ W/cm^2. Figure 5(a) presents the OFI EDF, compared with a Maxwellian EDF with the same average energy. It can be clearly seen that the OFI EDF extends to higher energies, yet has more electrons in the lower energy range, which enhances the recombination process. Figure 5(b) shows the calculated time-dependent gain. Time 0 is set when the peak of the ionizing beam reaches the plasma. The maximum gain is about 160 cm^{-1}. The above intensity, pulse duration, and pulse diameter at the focus would require a laser pulse with energy of about 150 mJ, which is available with current laser technology.

Figure 6 presents a compilation of the results obtained using the same parameters as for Fig. 5, but for several different pump beam diameters and hydrogen densities. Several interesting trends can be identified in the figure. First we see that in general, contrary to the results for Li III, the gain is smaller for tighter-focused pump beams. This is explained by the fact that on the one hand, the ponderomotive force becomes the main hurdle for gain, whereas the expansion cooling is not as important on the other hand. Next, we see that as the hydrogen density increases, the gain increases substantially, whereas the gain dependence upon the radius of the pump beam is quite weak. The latter is due to the strong, self-consistent electric field in the plasma for very high electron density, which prevents substantial space-charge separation and ponderomotive force heating. This also contributes to the higher gain, but the main contribution to the higher gain comes from the enhanced three-body recombination rate for higher electron density, as was discussed in the previous sections.

Another interesting parameter that has considerable influence on the gain in the high plasma density regime is

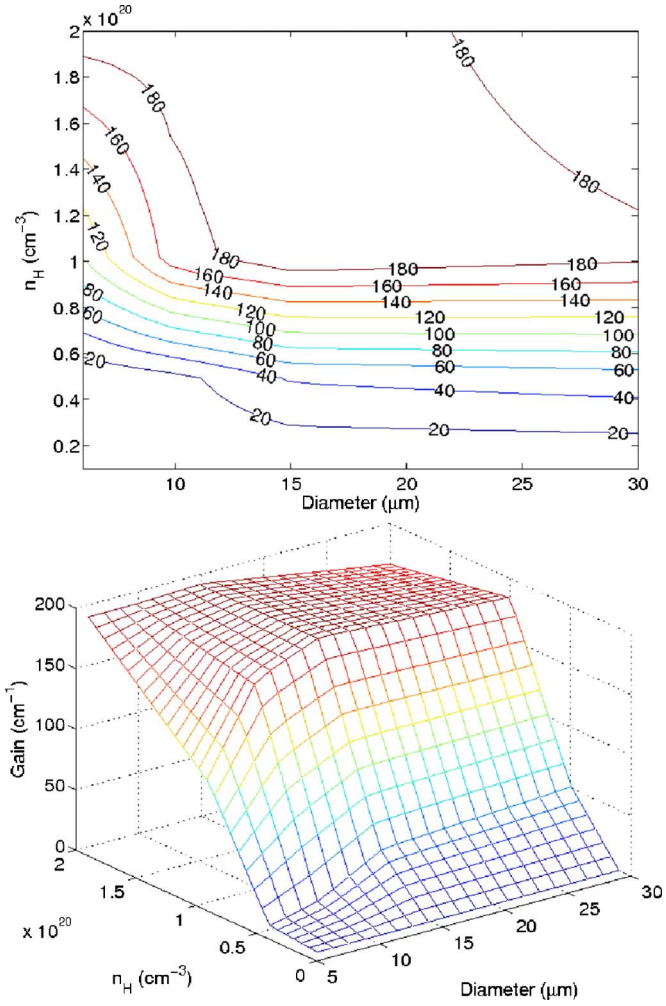

Fig. 6. (Color online) Compilation of the maximum gain coefficient achieved in CVI for different hydrogen densities and pump beam diameters. Both figures present the same data with different 3D visualization methods. The gain was calculated for the same plasma and pump laser parameters as Fig. 5, but for different hydrogen densities and pump beam diameters.

the pump laser pulse duration. Since the collision frequency is so high for this density, the amount of collisional heating is substantial, even for ultrashort pulses, and as mentioned above, collisional heating affects both

the H electrons and the C electrons. The variation of the gain with different the pump laser pulse durations is demonstrated in Fig. 7, which presents a compilation of results obtained for different pulse durations and different diameters of the pump laser, while all other parameters are the same as in Fig. 5. It is apparent that maximum gain is obtained for pulse duration $\tau \approx 20$ fs, and this gain is also less dependent on the beam diameter for this pulse duration. The intensity used was different for each pulse duration, in order to maintain full ionization. The ponderomotive force is generally higher for shorter pump pulses, i.e., shorter pulses require higher intensity to achieve full ionization. It seems that the maximum gain that appears for $\tau = 20$ fs is a result of the two competing processes: collisional heating, which is reduced when the pulse duration is shorter, and the ponderomotive force, which is enhanced when shorter pulses are being used. Evidence for this is the variation of the maximum gain with the pump beam diameter for a fixed pulse duration $[(\partial G_{\max}/\partial t)_\tau]$. It can be seen that for shorter pump pulses (with higher peak intensity), the maximum gain varies substantially with the pump beam diameter, and hardly any gain is predicted for very short, tightly focused, pulses. Therefore, although it may perhaps be easier experimentally to achieve the desired intensity by tightly focusing the pump beam, it is not necessarily beneficial to do so.

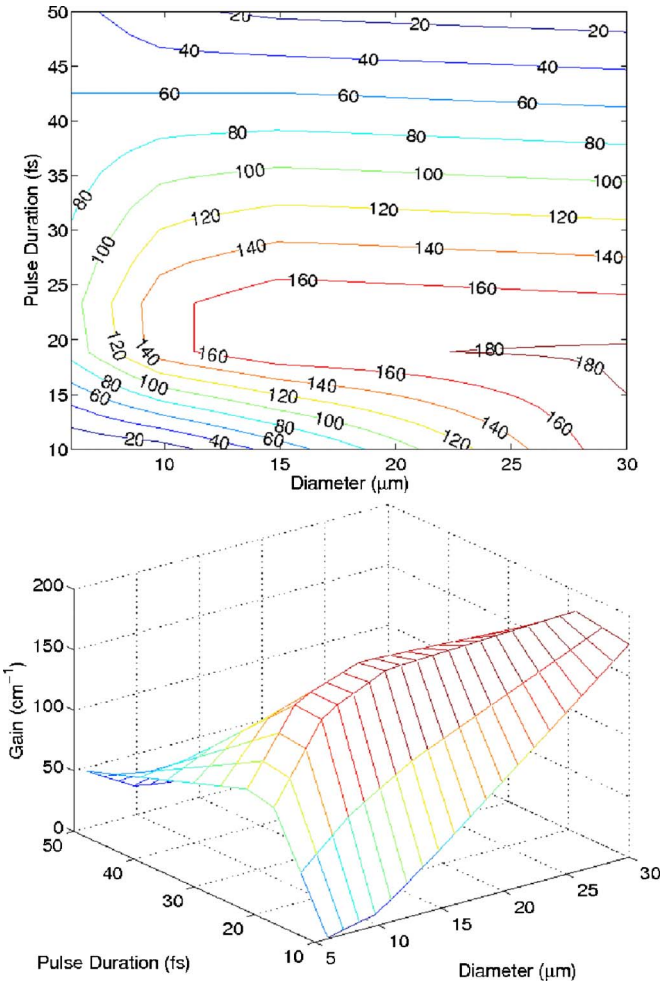

Fig. 7. (Color online) Compilation of the maximum gain coefficient achieved in C VI for different and pump beam durations and diameters. Both figures present the same data with different 3D visualization methods. All other parameters are the same as in Fig. 5. The pump peak intensities were different for different pulse durations to meet the requirement of full ionization. The intensities used are given in Table 1.

6. SUMMARY

Recombination gain in the transition to the ground state of hydrogenlike carbon, C VI ($2 \rightarrow 1$ transition at $\lambda = 3.4$ nm) was studied. We have shown that high gain (up to 180 cm^{-1}) is feasible to achieve with currently available university-size laser technology. We also analyzed the effects of different experimental parameters on the gain and pointed to the optimal parameters necessary for maximum gain to be generated. We note that some of the properties of the C VI case may, in fact, make it easier to achieve large recombination gain with this ion than with Li III. The calculated gain coefficient is much higher in this case, and, perhaps more importantly, the severe conditions on the pump beam diameter that were shown to limit the gain in the Li III case, do not apply here. Hence, larger diameter lasers could be used that would make it easier to propagate the pump beam for longer distances, achieve gain saturation, and get higher output energy. Finally, we have presented a feasible approach, relying on laser technologies that are currently available in university-type laboratories, to achieve a water-window table-top x-ray laser.

ACKNOWLEDGMENTS

We thank Ernest Valeo from PPPL for very useful discussions and Stephan Brunner from PPPL for the use of his FINDIFF FP solver. We also thank Goeff Pert (University of York, UK) for providing us with his recent paper (Ref. 27) prior to its publication. This work was supported by NSF (physics) fellowship and by a PU/PPPL Plasma Science and Technology fellowship.

Y. Avitzour can be reached via e-mail at avitzour@princeton.edu.

REFERENCES

1. J. Peyraud and N. Peyraud, "Population inversion in laser plasmas," J. Appl. Phys. **43**, 2993–2996 (1972).
2. W. Jones and A. Ali, "Theory of short-wavelength lasers from recombining plasmas," Appl. Phys. Lett. **26**, 450–451 (1975).
3. Y. Nagata, K. Midorikawa, S. Kubodera, M. Obara, H. Tashiro, and K. Toyoda, "Soft-x-ray amplification of the lyman-alpha transition by optical-field-induced ionization," Phys. Rev. Lett. **71**, 3774–3777 (1993).
4. K. M. Krushelnick, W. Tighe, and S. Suckewer, "X-ray laser studies of recombining lithium plasmas created by optical field ionization," J. Opt. Soc. Am. B **13**, 306–311 (1996).
5. D. V. Korobkin, C. H. Nam, S. Suckewer, and A. Goltsov, "Demonstration of soft x-ray lasing to ground state in Li III," Phys. Rev. Lett. **77**, 5206–5209 (1996).
6. A. Goltsov, A. Morozov, S. Suckewer, R. Elton, U. Feldman, K. Krushelnick, T. Jones, C. Moore, J. Seely, P. Sprangle, A. Ting, and A. Zigler, "Is efficiency of gain generation in Li III 13.5-nm laser with 0.25-μm subpicosecond pulses the

same as with 1 μm?" IEEE J. Sel. Top. Quantum Electron. **5**, 1453–1459 (1999).
7. N. H. Burnett and P. B. Corkum, "Cold-plasma production for recombination extreme-ultraviolet lasers by optical-field-induced ionization," J. Opt. Soc. Am. B **6**, 1195–1199 (1989).
8. K. A. Janulewicz, S. B. Healy, and G. J. Pert, "Hydrodynamics perspective on OFI-plasma x-ray lasers," Inst. Phys. Conf. Ser. **29**, 156–160 (1996).
9. K. A. Janulewicz, S. B. Healy, and G. J. Pert, "Modelling of OFI-plasma recombination X-ray lasers," Opt. Commun. **140**, 165–178 (1997).
10. G. J. Pert, "X-ray lasers pumped by ultra-short light pulses," J. Phys. IV **11**, 181–187 (2001).
11. Y. Avitzour, S. Suckewer, and E. Valeo, "Numerical investigation of recombination gain in the Li III transition to ground state," Phys. Rev. E **69**, 046409 (2004).
12. Y. Avitzour and S. Suckewer, "Numerical simulation of the effect of hydrogen on recombination gain in the transition to ground state of Li III," J. Opt. Soc. Am. B **23**, 925–931 (2006).
13. B. Smirnov and M. Chibisov, "Breaking up of atomic particles by an electric field and by electron collisions," Sov. Phys. JETP **22**, 585–592 (1966).
14. A. M. Perelomov, V. S. Popov, and M. V. Terent'ev, "Ionization of atoms in an alternating electric field," Sov. Phys. JETP **23**, 924–934 (1966).
15. P. Corkum, N. Burnett, and F. Brunel, "Above-threshold ionization in the long-wavelength limit," Phys. Rev. Lett. **62**, 1259–1262 (1989).
16. T. Ditmire, "Simulations of heating and electron energy distributions in optical field ionized plasmas," Phys. Rev. E **54**, 6735–6740 (1996).
17. Y. Ping, W. Cheng, S. Suckewer, D. Clark, and N. Fisch, "Amplification of ultrashort laser pulses by a resonant raman scheme in a gas-jet plasma," Phys. Rev. Lett. **92**, 175007 (2004).
18. W. Cheng, Y. Avitzour, Y. Ping, S. Suckewer, N. Fisch, M. Hur, and J. Wurtele, "Reaching the nonlinear regime of Raman amplification of ultrashort laser pulses," Phys. Rev. Lett. **94**, 045003 (2005).
19. C. Birdsall and A. Langdon, *Plasma Physics via Computer Simulation* (IOP, 2000).
20. E. M. Epperlein, "Fokker–Planck modeling of electron-transport in laser-produced plasmas," Laser Part. Beams **12**, 257–272 (1994).
21. S. Brunner and E. Valeo, "Simulations of electron transport in laser hot spots," Phys. Plasmas **9**, 923–936 (2002).
22. H. Griem, *Spectral Line Broadening by Plasmas* (Academic, 1974).
23. R. Elton, "Quasi-stationary population inversion on k-alpha-transitions," Appl. Opt. **14**, 2243–2249 (1975).
24. H. Griem, *Plasma Spectroscopy* (McGraw-Hill, 1964).
25. W. Lotz, "Electron-impact ionization cross-sections and ionization rate coefficients for atoms and ions from hydrogen to calcium," Z. Phys. **216**, 241–247 (1968).
26. V. Fisher, Y. Ralchenko, V. Bernshtam, A. Goldgirsh, Y. Maron, L. Vainshtein, and I. Bray, "Electron-impact-excitation cross sections of lithiumlike ions," Phys. Rev. A **56**, 3726–3733 (1997).
27. G. Pert, "Recombination and population inversion in plasmas generated by tunneling ionization," Phys. Rev. E **73**, 066401 (2006).